The NV metamaterial: Tunable quantum hyperbolic metamaterial using nitrogen vacancy centers in diamond

Qing Ai (艾清), Peng-Bo Li (李蓬勃), Wei Qin (秦伟), Jie-Xing Zhao (赵洁杏), C. P. Sun (孙昌璞), and Franco Nori

Phys. Rev. B **104**, 014109 — Published 21 July 2021

DOI: 10.1103/PhysRevB.104.014109

NV-Metamaterial: Tunable Quantum Hyperbolic Metamaterial Using Nitrogen-Vacancy Centers in Diamond

Qing Ai(艾清),[1,2] Peng-Bo Li(李蓬勃),[1,3] Wei Qin(秦伟),[1,4]
Jie-Xing Zhao(赵洁杏),[2] C. P. Sun(孙昌璞),[5] and Franco Nori[1,6]

[1] *Theoretical Quantum Physics Laboratory, RIKEN Cluster for Pioneering Research, Wako-shi, Saitama 351-0198, Japan*
[2] *Department of Physics, Applied Optics Beijing Area Major Laboratory, Beijing Normal University, Beijing 100875, China*
[3] *Department of Applied Physics, Xi'an Jiaotong University, Xi'an 710049, China*
[4] *Quantum Physics and Quantum Information Division, Beijing Computational Science Research Center, Beijing 100193, China*
[5] *Beijing Computational Science Research Center & Graduate School of Chinese Academy of Engineering Physics, Beijing 100084, China*
[6] *Department of Physics, The University of Michigan, Ann Arbor, Michigan 48109-1040, USA*

We show that nitrogen-vacancy (NV) centers in diamond can produce a novel quantum hyperbolic metamaterial. We demonstrate that a hyperbolic dispersion relation in diamond with NV centers can be engineered and dynamically tuned by applying a magnetic field at 20 K. This quantum hyperbolic metamaterial with a tunable window for the negative refraction allows for the construction of a superlens beyond the diffraction limit. In addition to subwavelength imaging, this NV-metamaterial can be used in spontaneous emission enhancement, heat transport and acoustics, analogue cosmology, and lifetime engineering. Therefore, our proposal interlinks the two hotspot fields, i.e., NV centers and metamaterials.

I. INTRODUCTION

Metamaterials with negative refraction have attracted broad interest [1–4]. Metamaterials can be used, e.g., for electromagnetic cloaking [5], perfect lens beyond diffraction limit [2], fingerprint identification in forensic science [6], simulating condensate matter phenomena [7] and reversed Doppler effect [8]. In order to realize negative refraction, sophisticated composite architectures [3, 9] and topologies [10–14] are fabricated to achieve simultaneously negative permittivity and permeability. However, hyperbolic (or indefinite) metamaterials were proposed [15–18] to overcome the difficulty of inducing a magnetic transition at the same frequency as the electric response. The magnetic response of double-negative metamaterials is so weak that it effectively shortens the frequency window of the negative refraction [10]. In addition to subwavelength imaging [19, 20] and focusing [20], hyperbolic metamaterials have been used to realize spontaneous emission enhancement [21], applied in heat transport [22] and acoustics [23], analogue cosmology [24], and lifetime engineering [25, 26].

On the other hand, quantum devices based on nitrogen-vacancy (NV) centers in diamond are under intense investigation [27, 28] as they manifest some novel properties and can be explored for many interesting applications [29, 30]. For example, NV centers in diamond have been proposed to realize a laser [31] and maser [32] at room temperature. Highly-sensitive solid-state gyroscopes [33] based on ensembles of NV centers in diamond can be realized by dynamical decoupling, to suppress the dipolar relaxation. Shortcuts to adiabaticity have been successfully performed in NV centers of diamond to initialize and transfer coherent superpositions [34, 35]. The high sensitivity to external signals makes single NV centers promising for quantum sensing of various physical parameters, such as electric field [36, 37], magnetic field [38–41], single electron and nuclear spin [42–50], and temperature [51–53]. Numerous hybrid quantum devices, composed of NV centers and other quantum systems, e.g. superconducting circuits and carbon nanotubes, have been proposed to realize demanding tasks [54–59].

Inspired by the rapid progress in both fields, here we propose to realize a hyperbolic metamaterial using NV centers in diamond. We consider an electric hyperbolic metamaterial, in which two principal components of its electric permittivity possess different signs. When an optical electromagnetic field around 637 nm induces the transition ${}^3A_2 \rightleftharpoons {}^3E$, the NV centers in diamond will negatively respond to the electric field in one direction. This process effectively modifies the relative permittivity of the diamond with NV centers and thus one principal component has a different sign. When a transverse magnetic (TH) mode is incident on this diamond with the principal axis of the negative component perpendicular to the interface, the transmitted light will be negatively refracted, as both the incident and transmitted light lie at the same side of the normal to the interface. Because this optical transition is intrinsically quantum and can *only* be described by quantum mechanics, we call it *quantum metamaterial*.

Note that it is difficult to fabricate classical metamaterials working in the optical-frequency domain, because the sizes of the elements therein are sub-micron. However, the NV centers in diamond can be easily fabricated in several ways [29], e.g., as an in-grown product of the chemical vapour deposition diamond synthesis process, as a product of radiation damage and annealing, as well as ion implantation and annealing in bulk and nanocrys-

talline diamond. The NV-metamaterials proposed here solve this problem.

This paper is organized as follows: In the next section, we briefly introduce the NV center in diamond, with the selection rules for optical transitions summarized in Appendix A, and the relative permittivity calculated by the linear-response theory, with details illustrated in Appendix B. We further prove in Appendix C that the bandwidth of the negative refraction is not significantly influenced if the Lorentz local-field theory is applied. Then, we show that we can switch between the negative and normal refraction by tuning the magnetic field in Sec. III. In Sec. IV, we elaborate how the negative refraction occurs. In Sec. V, we discuss experimental feasibility of our proposal. Finally, the main results are summarized in Sec. VI. In Appendix D, we prove that non-Hermitian Hamiltonian approach is equivalent to the quantum master equation approach and has been widely used to describe the damping and dephasing in open quantum systems.

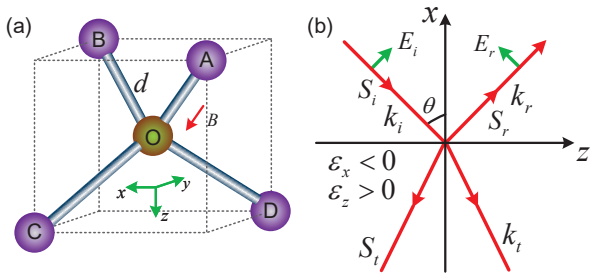

Figure 1. (a) Four possible orientations of NV centers in diamond [29, 68]: $\vec{r}_{\rm OA} = (-1,-1,-1)/\sqrt{3}$, $\vec{r}_{\rm OB} = (1,1,-1)/\sqrt{3}$, $\vec{r}_{\rm OC} = (1,-1,1)/\sqrt{3}$, $\vec{r}_{\rm OD} = (-1,1,1)/\sqrt{3}$. $d = 154$ pm is the length of carbon bond. The angle between any pair of the above four orientations is identically $\alpha = 109°28'$. The magnetic field $\vec{B}$ is along $-\vec{r}_{\rm OA}$. (b) Negative refraction for hyperbolic dispersion with $\varepsilon_x < 0$ and $\varepsilon_z > 0$. The TH mode is incident on the yz interface with electric field $\vec{E}_i$, wavevector $\vec{k}_i$, and Poynting vector $\vec{S}_i$. The angle between the normal (x-axis) and the incident field is θ. It is reflected with electric field $\vec{E}_r$, wavevector $\vec{k}_r$, and Poynting vector $\vec{S}_r$. The Poynting and wavevector of the transmitted wave are, respectively, $\vec{S}_t$ and $\vec{k}_t$.

II. MODEL

As schematically illustrated in Fig. 1(a), an NV center is composed of a vacancy, e.g. site O, and a substitutional nitrogen atom at one of its four possible neighboring sites, e.g. site A, B, C and D. The electronic ground state is a spin-triplet state with Hamiltonian [29]

$$\begin{aligned} H_{\rm gs} &= D_{\rm gs}S_z^2 + \mu_B g_{\rm gs}^{\parallel} B_z S_z + \mu_B g_{\rm gs}^{\perp}(B_x S_x + B_y S_y) \\ &\quad + d_{\rm gs}^{\parallel}\delta_z S_z^2 + d_{\rm gs}^{\perp}\delta_x\left(S_y^2 - S_x^2\right) \\ &\quad - d_{\rm gs}^{\perp}\delta_y\left(S_x S_y + S_y S_x\right), \end{aligned} \tag{1}$$

where $D_{\rm gs} = 2.88$ GHz is the zero-field splitting of the electronic ground state, μ_B is the Bohr magneton, $g_{\rm gs}^{\parallel} \simeq g_{\rm gs}^{\perp} = g_{\rm gs} \simeq 2$ are respectively the components of the g-factor of the electronic ground state, $\vec{B} = B_x\hat{e}_x + B_y\hat{e}_y + B_z\hat{e}_z$ is the magnetic field, S_α ($\alpha = x, y, z$) are the spin-1 operators for the electron spin, $\vec{\delta} = \delta_x\hat{e}_x + \delta_y\hat{e}_y + \delta_z\hat{e}_z$ is the strain field, $d_{gs}^{\perp} = 17$ Hz cm/V and $d_{gs}^{\parallel} = 0.35$ Hz cm/V [60] are the components of the ground-state electric dipole moment.

At low temperatures, the Hamiltonian of the electronic excited state is given as [29]

$$\begin{aligned} H_{\rm es} &= D_{\rm es}^{\parallel} S_z^2 - \lambda_{\rm es}^{\parallel}\sigma_y \otimes S_z \\ &\quad + D_{\rm es}^{\perp}[\sigma_y \otimes (S_y^2 - S_x^2) - \sigma_x \otimes (S_y S_x + S_x S_y)] \\ &\quad + \lambda_{\rm es}^{\perp}[\sigma_z \otimes (S_x S_z + S_z S_x) - \sigma_x \otimes (S_y S_z + S_z S_y)] \\ &\quad + \mu_B(l_{\rm es}^{\parallel}\sigma_y + g_{\rm es}^{\parallel} S_z)B_z + \mu_B g_{\rm es}^{\perp}(S_x B_x + S_y B_y) \\ &\quad + d_{\rm es}^{\parallel}\delta_z\sigma_y + d_{\rm es}^{\perp}\delta_x\sigma_z - d_{\rm es}^{\perp}\delta_y\sigma_x, \end{aligned} \tag{2}$$

where σ_x, σ_y and σ_z are the Pauli matrices. The values of the fine structure parameters are obtained from the direct observation as [61] $D_{\rm es}^{\parallel} = 1.42$ GHz, $D_{\rm es}^{\perp} = 0.76$ GHz, $\lambda_{\rm es}^{\perp} = 5.3$ GHz and $\lambda_{\rm es}^{\parallel} = 0.14$ GHz. The magnetic circular dichroism is given as $l_{\rm es}^{\parallel} = 0.1$ [62, 63]. The components of the excited-state g-factor tensor are $g_{\rm es}^{\parallel} = g_{\rm es}^{\perp} = 2.01$ [64, 65]. The components of the electric dipole moment are $d_{\rm es}^{\parallel}, d_{\rm es}^{\perp} \approx 6$ kHz m/V [66, 67]. Because $d_{\rm es}^{\parallel}$ and $d_{\rm es}^{\perp}$ are larger than $d_{\rm gs}^{\parallel}$ and $d_{\rm gs}^{\perp}$ by 5 orders of magnitude, the spectra of the excited-states are more sensitive to the strain field.

As illustrated in Fig. 1(a), there are four possible orientations for the NV centers in diamond [27–30, 68]. Since both Hamiltonians of the ground and excited states are obviously dependent on the relative orientation of the symmetry axis with respect to the magnetic field, the energy spectra and thus the electromagnetic response of the NV centers to the applied fields are different for the four possible orientations.

According to Appendix A, the non-zero transition matrix elements of the position vector $\vec{r} = x\hat{e}_x + y\hat{e}_y + z\hat{e}_z$ are in the following transitions $|\Phi^c_{A_2;S,m_s}\rangle \overset{\alpha'}{\rightleftharpoons} |\Phi^c_{E,\alpha;S,m_s}\rangle$ [69], where $\alpha, \alpha' = x, y$ and $\alpha \neq \alpha'$. For the ground states, they can be formally diagonalized as $|g_i\rangle = \sum_{j=-1}^{1} C_{ij}^g |\Phi^c_{A_2;1,j}\rangle$ ($i = 1, 2, 3$) with eigenenergy E_i^g. And for the excited states, they can be formally diagonalized as $|e_f\rangle = \sum_{\alpha=x,y}\sum_{j=-1}^{1} C_{f\alpha j}^e |\Phi^c_{E,\alpha;1,j}\rangle$ ($f = 1, 2, \cdots, 6$) with eigenenergy E_f^e. Notice that the degeneracy of the electronic excited states is lifted for different α's at low temperatures. According to Refs. [70, 71], the constitutive relation reads $\vec{D} = \varepsilon_0 \overleftrightarrow{\varepsilon}_r \vec{E} = \varepsilon_{\rm D}\varepsilon_0\vec{E} + \vec{P}$, where $\vec{D}$ is the electric displacement, ε_0 is the electric permittivity of vacuum, $\overleftrightarrow{\varepsilon}_r$ and $\varepsilon_{\rm D}$ are, respectively, the relative permittivity tensor of diamond with and without NV centers. The polarization density can be calculated using the linear-response theory [10, 72], cf. Appendix B,

as

$$\vec{P} = -\frac{1}{\hbar v_0}\mathrm{Re}\left[\sum_{j,i,f}{}' \rho_i \frac{\vec{d}_{if}^{(j)}\left(\vec{d}_{fi}^{(j)}\cdot\vec{E}\right)}{\omega-\Delta_{fi}^{(j)}+i\gamma}\right], \tag{3}$$

where $\hbar$ is the Planck constant, $n_0 = v_0^{-1}$ is the density of the NV centers, ρ_i is the probability of the initial state $|g_i\rangle$ at thermal equilibrium, i.e., $\rho(0) = \sum_i \rho_i |g_i\rangle\langle g_i|$, ω is the frequency of the electric field $\vec{E} = \vec{E}_0\cos(\omega t)$, $\Delta_{fi}^{(j)}$ is the transition frequency of the jth NV center between the initial state $|g_i\rangle$ and the final state $|e_f\rangle$, γ^{-1} is the lifetime of the final state, and $\vec{d}_{if}^{(j)}$ is the transition matrix element of the electric dipole of the jth NV center between the initial and final states. The prime over the summation indicates that $i \neq f$.

The relative permittivity tensor is

$$\overleftrightarrow{\varepsilon}_r = \varepsilon_{\mathrm{D}} - \sum_{j,i,f}{}' \sum_{j_1,j_2} \mathrm{Re}\left[\frac{(C_{fxj_1}^{e(j)}\vec{d}_y^{(j)} + C_{fyj_1}^{e(j)}\vec{d}_x^{(j)})}{3\hbar\varepsilon_0 v_0(\omega-\Delta_{fi}^{(j)}+i\gamma)} \times C_{ij_1}^{g(j)*}C_{ij_2}^{g(j)}(C_{fxj_2}^{e(j)*}\vec{d}_y^{(j)} + C_{fyj_2}^{e(j)*}\vec{d}_x^{(j)})\right], \tag{4}$$

where $\vec{d}_x^{(j)}$ and $\vec{d}_y^{(j)}$ are the components of the transition dipole of the jth NV center. Clearly, there can be eighteen possible negative permittivity components around the eighteen transition frequencies $\Delta_{fi}^{(j)} = E_f^{e(j)} - E_i^{g(j)}$ of the jth NV center. However, if a static magnetic field is applied along the direction $(1,1,1)$, all transition frequencies would be identical for all orientations except the one along $\vec{r}_{\mathrm{OA}}$ [68]. Moreover, the relative permeability is not modified by the presence of NV centers because the transition ${}^3A_2 \rightleftharpoons {}^3E$ can only be induced by the electric-dipole couplings to the electromagnetic field [29]. In the above calculations, we assume isolated identical NV centers for simplicity. Generally, there are dipole-dipole interactions between the NV centers and inhomogeneous strain fields on different NV centers [29]. Due to the presence of the inhomogeneous strain fields, the NV centers are different. However, the dipole-dipole interaction can be neglected as long as the dipole-dipole interaction is much smaller than inhomogeneity induced by the random strain field. In Ref. [73], a dipole-dipole interaction with 420 kHz is reported for the density of NV centers with 45 ppm. For $n_0 = 0.5$ ppm, the dipole-dipole interaction is estimated as 4.67 kHz since it scales linearly to n_0. As long as the standard deviation of the random strain field is much larger than 4.67 kHz, the dipole-dipole interaction can be reasonably neglected, which will be investigated in the next section.

III. QUANTUM SWITCH OF NEGATIVE REFRACTION AND NORMAL REFRACTION

In order to show that the negative refraction can be switched on/off, we will analyze the effect of the magnetic field on the energy spectra of NV centers. According to Eq. (4), the permittivity might be negative around the transition frequencies. When $\vec{B}$ is in the direction of $(1,1,1)$, the NV centers of orientations along $\vec{r}_{\mathrm{OB}}$, $\vec{r}_{\mathrm{OC}}$, $\vec{r}_{\mathrm{OD}}$ are identical, while the NV centers of orientation along $\vec{r}_{\mathrm{OA}}$ are different, which makes the material anisotropic. Generally, there are thirty-six transition frequencies Δ_{fi}, which can be subtly tuned by varying the magnetic field. Figure 2 shows the regions of negative refraction in the frequency domain vs different magnetic field B's. When $B = 0$ G, since all four possible orientations of the NV centers are identical, the three eigenvalues of permittivity possess the same sign and thus negative refraction is absent. However, if a non-vanishing B is introduced, we would expect negative refraction in some frequency domains. For example, when $B = 10^3$ G, the negative refraction can be realized around $\Delta_{ij} \simeq 0.2$ GHz, which can not be observed for $B = 0$ G. We remark that the increasing magnetic field does not only modify the transition frequencies, but also redistributes electric dipoles among the eigenstates. In this regard, by tuning the magnetic field, we can switch on/off the negative refraction on demand. Here, the density of NV centers in diamond is 0.5 ppm and $\gamma = 50$ MHz at $T = 20$ K [74].

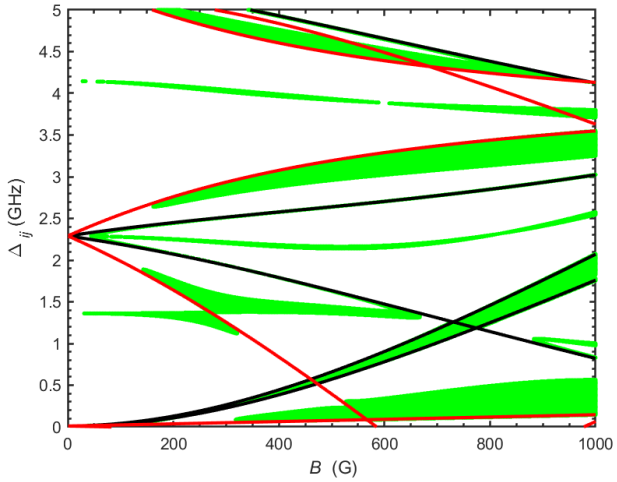

Figure 2. The negative refraction (green shadows) vs $\Delta_{ij} = E_i^e - E_j^g - 1.945$ eV and B when the magnetic field is applied along the direction of (1,1,1). The transition frequencies are identical and denoted by black curves for the NV centers of orientations along $\vec{r}_{\mathrm{OB}}$, $\vec{r}_{\mathrm{OC}}$, $\vec{r}_{\mathrm{OD}}$ in Fig. 1(a) due to the special choice of $\vec{B}$. The transition frequencies for the NV centers of orientation along $\vec{r}_{\mathrm{OA}}$ are different and denoted by red curves . The density of NV centers is $n_0 = 0.5$ ppm and the decay rate of the excited state is $\gamma = 50$ MHz at $T = 20$ K [74].

Generally speaking, the NV centers in diamond are not in a perfect crystal and thus are exposed to strain fields. Since the eigenenergies and eigenstates are dependent on the strain field, for simplicity, we consider a random strain field in the x-direction of normal distribution, with mean $\overline{\delta} = 0.83$ MV/m and standard deviation σ_δ. Since

the mean shifts the energy spectra of the ensemble homogeneously, we investigate the dependence of the bandwidth of the negative refraction on σ_δ in Fig. 3. When the strain fields experienced by different NV centers are almost homogeneous, i.e., σ_δ is small, the bandwidth is nearly not influenced by the strain field. However, as σ_δ increases, the bandwidth is effectively narrowed as the negative response of different NV centers do not overlap at the same frequency region. Eventually, the negative refraction will disappear for a sufficiently-large inhomogeneous strain field.

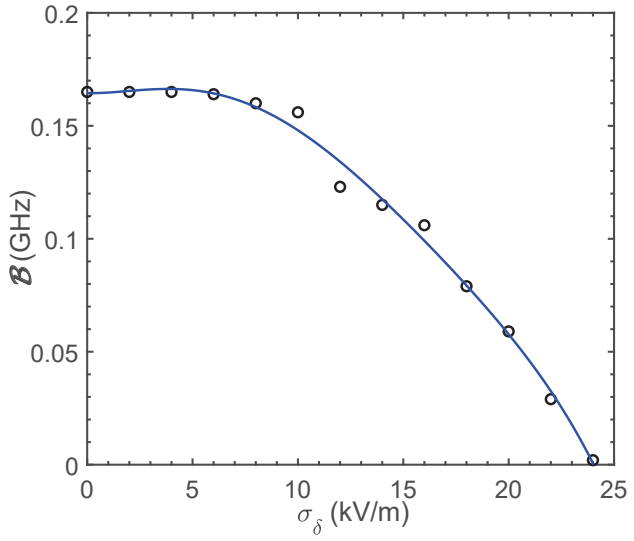

Figure 3. The bandwidth of the negative refraction $\mathcal{B}$ vs σ_δ for $\overline{\delta} = 1$ MV/m, $n_0 = 0.5$ ppm, $B = 800$ G, and $T = 20$ K. Here, we assume the ensemble of NV centers are exposed to random strain fields of normal distribution with mean $\overline{\delta}$ and standard deviation σ_δ.

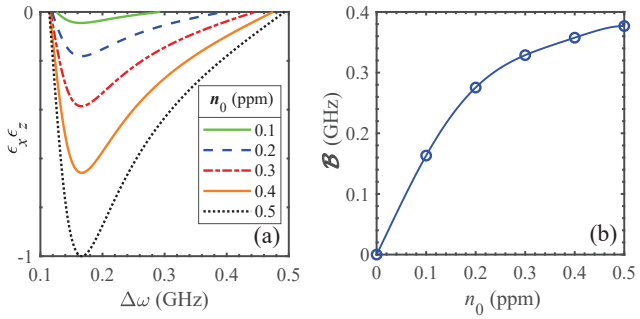

Figure 4. The dependence of negative refraction on the density of NV centers n_0. (a) The product of two components of permittivity tensor $\varepsilon_x\varepsilon_z$ vs detuning $\Delta\omega = \omega - \Delta_{fi}$; (b) The bandwidth $\mathcal{B}$ vs n_0. The intensity of magnetic field is $B = 800$ G. Other parameters are $d_x = d_y = 11$ D [75], $\gamma = 50$ MHz at $T = 20$ K [74], $\varepsilon_{\rm D} = 5.7$ [76], and $\mu_{\rm D} = 1 - 2.1 \times 10^{-5}$ [77].

As implied by Eq. (4), the negative eigenvalue of the permittivity can be more pronounced if there are more NV centers in a given diamond. Figure 4(a) shows the bandwidth of the negative refraction for different densities of NV centers, as determined by $\varepsilon_x\varepsilon_x < 0$, which are the two components of the diagonalized permittivity tensor

$$\overleftrightarrow{\varepsilon_r} = \begin{pmatrix} \varepsilon_x & 0 & 0 \\ 0 & \varepsilon_y & 0 \\ 0 & 0 & \varepsilon_z \end{pmatrix}. \tag{5}$$

Compared to the situation with $n_0 = 0.1$ ppm, the window of the negative refraction for $n_0 = 0.5$ ppm has been significantly broadened, because more NV centers can negatively respond to the applied electromagnetic field. With this increased density, the negative dip at $\Delta\omega = 0.2$ GHz can be more profound for $B = 800$ G. However, the bandwidth will converge as the density increases. Notice that in the numerical simulations we have not used the local-field correction [70, 71], since it will not substantially change the center and bandwidth of the negative refraction domain but modify the magnitude of the permittivity [10, 78, 79], as also proven in Appendix C. Therefore, we have demonstrated the negative refraction in diamond with NV centers.

IV. NEGATIVE REFRACTION

In Ref. [1], it has been shown that for a double-negative metamaterial there can be negative refraction. However, in the NV centers of diamond, because the electric permittivity tensor possesses two different components, it is natural to ask whether negative refraction can exist. Below, we will demonstrate that negative refraction can indeed occur for a TH incident mode, cf. Fig. 1(b).

According to Maxwell's equations [70, 71], $\nabla \times \vec{E} = -\frac{\partial}{\partial t}\mu_{\rm D}\vec{H}$, $\nabla \times \vec{H} = \frac{\partial}{\partial t}\overleftrightarrow{\varepsilon}\vec{E}$, where both the current density and the charge density vanish, $\overleftrightarrow{\varepsilon} = \varepsilon_0\overleftrightarrow{\varepsilon_r}$ is the permittivity of diamond with NV centers, and $\mu_{\rm D}$ is the permeability of pure diamond.

Assuming that the transmitted electric and magnetic fields are, respectively, $\vec{E}_t(\vec{r},t) = (E_{tx}\hat{e}_x + E_{tz}\hat{e}_z)\exp[i(\vec{k}_t\cdot\vec{r}-\omega t)]$, $\vec{H}_t(\vec{r},t) = H_{ty}\hat{e}_y\exp[i(\vec{k}_t\cdot\vec{r}-\omega t)]$, we have

$$(\nabla\times\nabla\times\overleftrightarrow{I} - \mu_0\omega^2\overleftrightarrow{\varepsilon})\vec{E}_t = 0, \tag{6}$$

where $\overleftrightarrow{I}$ is the identity dyadic. For nontrivial solutions, the dispersion relation for the extraordinary mode reads

$$\varepsilon_x k_{tx}^2 + \varepsilon_z k_{tz}^2 = \mu_0\omega^2\varepsilon_x\varepsilon_z, \tag{7}$$

assuming $k_y = 0$. Such a dispersion relation for the extraordinary mode is hyperbolic or indefinite because $\varepsilon_x\varepsilon_z < 0$.

According to the boundary condition [70], the tangential components of the wavevector across the interface should be equal, i.e., $k_{tz} = k_{iz} > 0$, $k_{tx} = k_{ix}$. By inserting Eq. (7) into Eq. (6), we obtain the relation between

E_{tx} and E_{tz} as $\varepsilon_x k_{tx} E_{tx} + \varepsilon_z k_{tz} E_{tz} = 0$. By Maxwell equations, we have

$$\vec{H} = -\frac{\omega \varepsilon_z E_{tz}}{k_{tx}} \hat{e}_y \exp\left[i\left(\vec{k}_t \cdot \vec{r} - \omega t\right)\right]. \tag{8}$$

The time-averaged Poynting vector reads [70] $\vec{S}_t = \frac{1}{2}\mathrm{Re}(\vec{E}_t \times \vec{H}_t^*)$, with the components being $S_{tx} = \frac{\omega \varepsilon_z}{2k_{tx}} E_{tz}^2$, $S_{tz} = \frac{\varepsilon_x \omega E_{tx}^2}{2k_{tz}} < 0$, because $\varepsilon_x < 0$ and $\omega, k_{tz} > 0$. In order to transmit energy from the interface into the medium, S_{tx} should be negative and thus $k_{tx} < 0$ as $\omega, \varepsilon_z > 0$. Together with Eq. (7), we have

$$k_{tx} = -k_i \sqrt{\frac{\varepsilon_z}{\varepsilon_0}\left(1 - \frac{\varepsilon_0}{\varepsilon_x}\sin^2\theta\right)}, \tag{9}$$

where $k_i^2 = \mu_0 \varepsilon_0 \omega^2$. Because $S_{tx}, S_{tz} < 0$, we have proven that for a uniaxial crystal with hyperbolic dispersion, the negative refraction exists for a TH incident field.

V. EXPERIMENTAL FEASIBILITY

In order to analyze experiment feasibility by simple calculation, we consider that all NV centers are aligned in the same direction, which is within the state-of-art technology [80]. We further assume no strain field is considered to obtain an analytic result. For zero magnetic field, the Hamiltonians of the electronic ground and excited states are further simplified as $H_{\mathrm{gs}} = D_{\mathrm{gs}} \sum_{m_z=\pm 1} |\Phi^c_{A_2;1,m_z}\rangle\langle\Phi^c_{A_2;1,m_z}|$ and $H_{\mathrm{es}} \simeq \sum_{\alpha=x,y} \sum_{m_z=\pm 1} D^{\parallel}_{\mathrm{es}} |\Phi^c_{E,\alpha;1,m_z}\rangle\langle\Phi^c_{E,\alpha;1,m_z}|$, cf. Appendix A, where we have omitted the strain-related coupling.

For simplicity, the orientations of all NV centers are assumed to be along the z-axis. Thus, all matrix elements of the transition electric dipole are equal to $\vec{d}_{if} = \langle\Phi^c_{A_2;1,m_z}|\vec{d}|\Phi^c_{E,\alpha;1,m_z}\rangle = 11(\hat{e}_x + \hat{e}_y)$ D [75]. Initially, the NV centers are in the thermal state $\rho(0) = \frac{1}{3}\sum_{m_z} |\Phi^c_{A_2;S,m_s}\rangle\langle\Phi^c_{A_2;S,m_s}|$. Therefore,

$$\vec{P} = -2\zeta\gamma\varepsilon_0 \mathrm{Re}\left[\frac{(\hat{e}_x\hat{e}_x + \hat{e}_y\hat{e}_y + \hat{e}_x\hat{e}_y + \hat{e}_y\hat{e}_x)\vec{E}}{\omega - \Delta_{fi} + i\gamma}\right], \tag{10}$$

where $\zeta = \frac{242 n_0\ \mathrm{D}^2}{9\hbar\gamma\varepsilon_0}$. The three principal components of the relative permittivity are, respectively,

$$\varepsilon_r^{(1)} = \varepsilon_{\mathrm{D}} - \frac{2\zeta\gamma(\omega - \Delta_{fi})}{(\omega - \Delta_{fi})^2 + \gamma^2}, \tag{11}$$

$\varepsilon_r^{(2)} = \varepsilon_r^{(3)} = \varepsilon_{\mathrm{D}}$. When the frequency of the incident field is $\omega = \Delta_{fi} + \gamma$, one principal component can be negative if $n_0 > n_0^c = 1.77 \times 10^{21}\ \mathrm{m}^{-3}$, while the other principal components remain positive. Because two carbon atoms occupy a volume $v = (1.78 \times 10^{-10})^3\ \mathrm{m}^{-3}$, the minimum density of the NV centers to demonstrate negative refraction is

$$\frac{1}{2} v n_0^c = 5.00\ \mathrm{ppb}, \tag{12}$$

which is feasible in experimental fabrication, e.g. 16 ppm [81]. In addition, as can be proven, the negative component of permittivity appears in the z-axis, because of $\vec{B} \parallel \vec{e}_z$ and the symmetry of four possible orientations of the NV centers.

In the above calculation, in order to analytically obtain the minimum density of NV centers for negative refraction, we assume a simple model in which all NV centers are aligned in the same direction and the strain field is absent. However, in a practical sample, NV centers are possible in all four directions and the strain fields perceived by individual NV centers are random due to different distances to the surface and defects nearby. By numerical simulations, we can show that in the presence of random strain field with r.m.s. being about 1.6 MHz [82], the negative refraction can be observed as long as the density of NV centers is larger than 141 ppb. Although this is larger than the counterpart obtained by the above simplified model by one order, these two results are qualitatively consistent with each other. Furthermore, the dipole-dipole interaction between adjacent NV centers, about 1.316 kHz for 141 ppb, can be reasonably neglected since it only leads to energy shift due to the large detuning induced by the random strain field. Therefore, by the analytical and numerical calculations, we show that the negative refraction in diamond with NV centers can be present.

VI. CONCLUSIONS

In this work, we proposed a new approach to realize hyperbolic metamaterial using diamond with NV centers in the optical frequency regime. Because of the long lifetime of the excited states of the NV centers, this hyperbolic metamaterial manifests an intriguing window for negative refraction. By varying the applied magnetic field to tune the energy spectra of both ground and excited states, the frequency of the negative refraction can be tuned in a wide range. Note that it is difficult to fabricate classical metamaterials working in optical-frequency domain, because the sizes of the elements therein are submicron. The NV-metamaterials proposed here solve this problem. Because this NV-metamaterial can be used in subwavelength imaging, spontaneous emission enhancement, heat transport and acoustics, analogue cosmology, and lifetime engineering, our proposal bridges the gap between NV centers and metamaterials.

ACKNOWLEDGMENTS

We thank stimulating discussion with Zhou Li and K. Y. Bliokh. This work was supported by NTT Research, Army Research Office (ARO) (Grant No. W911NF-18-1-0358), Japan Science and Technology Agency (JST) (via the CREST Grant No. JPMJCR1676), Japan Society for the Promotion of Science (JSPS) (via the KAKENHI Grant No. JP20H00134 and the JSPS-RFBR Grant No. JPJSBP120194828), the Asian Office of Aerospace Research and Development (AOARD) (via Grant No. FA2386-20-1-4069), and the Foundational Questions Institute Fund (FQXi) via Grant No. FQXi-IAF19-06. Q.A. was partially supported by NSFC under Grant Nos. 11674033, 11505007, 11474026, and Beijing Natural Science Foundation under Grant No. 1202017.

Appendix A: Selection Rules of Optical Transitions

According to Ref. [83], there are four outer electrons distributed in the a_1, e_x and e_y levels, i.e., $a_1^2e^2$. On account of the spin degree of freedom, the electronic ground states can be written in the second quantization form, i.e., $|a_1\bar{a}_1e_x\bar{e}_xe_y\bar{e}_y\rangle$ with an overbar denoting spin-down, as

$$\begin{aligned}
|\Phi^c_{A_2;1,0}\rangle &= \frac{1}{\sqrt{2}}(|111001\rangle + |110110\rangle),\\
|\Phi^c_{A_2;1,1}\rangle &= |111010\rangle,\\
|\Phi^c_{A_2;1,-1}\rangle &= |110101\rangle,
\end{aligned} \tag{A1}$$

where the superscript c means configuration, the subscripts are ordered as $j,k;S,m_s$ with j being the irreducible representation, k being the row of irreducible representation, S being the total spin and m_s being the spin projection along the symmetry axis of the NV center. The six first excited states, i.e., a_1e^3, are respectively

$$\begin{aligned}
|\Phi^c_{E,x;1,0}\rangle &= \frac{1}{\sqrt{2}}(|100111\rangle + |011011\rangle),\\
|\Phi^c_{E,y;1,0}\rangle &= \frac{1}{\sqrt{2}}(|101101\rangle + |011110\rangle),\\
|\Phi^c_{E,x;1,1}\rangle &= |101011\rangle,\\
|\Phi^c_{E,y;1,1}\rangle &= |101110\rangle,\\
|\Phi^c_{E,x;1,-1}\rangle &= |010111\rangle,\\
|\Phi^c_{E,y;1,-1}\rangle &= |011101\rangle.
\end{aligned} \tag{A2}$$

By comparing Eq. (A1) and (A2), we notice that there is one electron transiting from a_1 orbital to e orbital. In the absence of spin-orbital coupling, on account of conservation of spin and total angular momentum [84], the transitions, i.e., $|\Phi^c_{A_2;1,m_s}\rangle \rightleftharpoons |\Phi^c_{E,\alpha;1,m_s}\rangle$ with $m_s = 0,\pm1$ and $\alpha = x,y$, are allowed by the electric-dipole coupling. The non-zero transition matrix elements of the position vector $\vec{r} = x\hat{e}_x + y\hat{e}_y + z\hat{e}_z$ with $\hat{e}_i$ unit vector along direction $i = x,y,z$ are listed as [69]

$$\begin{aligned}
&\langle a_1|x|e_x\rangle \neq 0,\\
&\langle a_1|y|e_y\rangle \neq 0,\\
&\langle e_y|x|e_y\rangle = \langle e_x|y|e_y\rangle = -\langle e_x|x|e_x\rangle \neq 0.
\end{aligned} \tag{A3}$$

Therefore, the selection rules for optical transitions are

$$|\Phi^c_{A_2;S,m_s}\rangle \overset{\alpha'}{\rightleftharpoons} |\Phi^c_{E,\alpha;S,m_s}\rangle, \tag{A4}$$

where $\alpha,\alpha' = x,y$ with $\alpha' \neq \alpha$ indicates the polarization of the electric field.

As shown in Fig. 1(a), there are four possible symmetry axes for the NV centers in diamond, i.e., $\vec{r}_{\rm OA} = (-1,-1,-1)/\sqrt{3}$, $\vec{r}_{\rm OB} = (1,1,-1)/\sqrt{3}$, $\vec{r}_{\rm OC} = (1,-1,1)/\sqrt{3}$, and $\vec{r}_{\rm OD} = (-1,1,1)/\sqrt{3}$. Here, $\vec{r}_{\rm OA}$ can be obtained by rotating the z-axis around the axis $\vec{n}_{\rm OA} = (-1,1,0)/\sqrt{2}$ by an angle $\theta_{\rm OA} = -(180^\circ - \alpha/2)$, i.e.,

$$\vec{r}_{\rm OA} = R(\vec{n}_{\rm OA},\theta_{\rm OA})\hat{e}_z = R(\vec{n}_{\rm OA},\theta_{\rm OA})(0,0,1)^T, \tag{A5}$$

where the rotation matrix around $\vec{n} = (n_x,n_y,n_z)$ by an angle θ is [85]

$$R(\vec{n},\theta) = \begin{pmatrix} R_{11} & R_{12} & R_{13}\\ R_{21} & R_{22} & R_{23}\\ R_{31} & R_{32} & R_{33}\end{pmatrix} \tag{A6}$$

with

$$\begin{aligned}
R_{11} &= \cos\theta + n_x^2(1-\cos\theta),\\
R_{12} &= n_xn_y(1-\cos\theta) - n_z\sin\theta,\\
R_{13} &= n_xn_z(1-\cos\theta) + n_y\sin\theta,\\
R_{21} &= n_xn_y(1-\cos\theta) + n_z\sin\theta,\\
R_{22} &= \cos\theta + n_y^2(1-\cos\theta),\\
R_{23} &= n_yn_z(1-\cos\theta) - n_x\sin\theta,\\
R_{31} &= n_xn_z(1-\cos\theta) - n_y\sin\theta,\\
R_{32} &= n_yn_z(1-\cos\theta) + n_x\sin\theta,\\
R_{33} &= \cos\theta + n_z^2(1-\cos\theta).
\end{aligned} \tag{A7}$$

And $\vec{r}_{\rm OB}$ can be obtained by rotating the z-axis around the axis $\vec{n}_{\rm OA} = (-1,1,0)/\sqrt{2}$ by an angle $-\theta_{\rm OA}$, i.e.,

$$\vec{r}_{\rm OB} = R(\vec{n}_{\rm OA},-\theta_{\rm OA})\hat{e}_z. \tag{A8}$$

$\vec{r}_{\rm OC}$ can be obtained by rotating the z-axis around the axis $\vec{n}_{\rm OC} = (1,1,0)/\sqrt{2}$ by an angle $\theta_{\rm OC} = \alpha/2$, i.e.,

$$\vec{r}_{\rm OC} = R(\vec{n}_{\rm OC},\theta_{\rm OC})\hat{e}_z. \tag{A9}$$

$\vec{r}_{\rm OD}$ can be obtained by rotating the z-axis around the axis $\vec{n}_{\rm OC} = (1,1,0)/\sqrt{2}$ by an angle $-\theta_{\rm OC}$, i.e.,

$$\vec{r}_{\rm OD} = R(\vec{n}_{\rm OC},-\theta_{\rm OC})\hat{e}_z. \tag{A10}$$

Appendix B: Linear-Response Theory

In order to simulate the electromagnetic response of the diamond with NV centers in the presence of applied fields, we can employ the linear-response theory [72] to calculate the electric permittivity. When there is an electric field applied, the NV center is polarized as

$$\langle\vec{d}\rangle = \int \frac{d\omega}{2\pi} S(\omega)\vec{E}(\omega)e^{-i\omega t}, \tag{B1}$$

where the Fourier transform of the time-dependent electric field $\vec{E}(t) = \vec{E}_0 \cos\Omega t$ with amplitude $\vec{E}_0$ and frequency Ω is

$$\vec{E}(\omega) = \int_{-\infty}^{\infty} dt\ \vec{E}(t)e^{i\omega t}, \tag{B2}$$

$$S(\omega) = -J(\omega) - J^*(-\omega). \tag{B3}$$

Here, $J(\omega)$ is the Fourier transform of the dipole-dipole correlation function, i.e.,

$$J(\omega) = -i\int_0^{\infty} dt\ \mathrm{Tr}[\vec{d}(t)\vec{d}\rho(0)]e^{i\omega t}, \tag{B4}$$

where the initial state of the NV center is

$$\rho(0) = \sum_i \rho_i |i\rangle\langle i| \tag{B5}$$

with $\sum_i \rho_i = 1$.

The electric dipole in the Heisenberg picture is

$$\vec{d}(t) = \exp(iH^\dagger t/\hbar)\vec{d}\exp(-iHt/\hbar), \tag{B6}$$

where the total Hamiltonian including the manifold of the electronic ground and excited states is

$$H = H_{\mathrm{es}} \otimes |e\rangle\langle e| + H_{\mathrm{gs}} \otimes |g\rangle\langle g|, \tag{B7}$$

with $|g\rangle$ ($|e\rangle$) being the electronic ground (excited) state. Because the Fourier transform of the electric field can be rewritten as

$$\vec{E}(\omega) = \pi\vec{E}_0[\delta(\omega+\Omega) + \delta(\omega-\Omega)], \tag{B8}$$

the electric dipole of the NV center in the applied electric field is

$$\langle\vec{d}\rangle = -\vec{E}_0\mathrm{Re}\{[J(\Omega) + J^*(-\Omega)]\, e^{-i\Omega t}\}, \tag{B9}$$

where

$$J(\omega) = \sum_{i,f}{}' \frac{\rho_i \vec{d}_{if}\vec{d}_{fi}}{\omega - \Delta_{fi} + i\gamma}. \tag{B10}$$

Using the non-Hermitian Hamiltonian in Appendix D,

$$H_i = \langle i|\, H\, |i\rangle = E_i - \frac{i}{2}\gamma \tag{B11}$$

with $-i\gamma/2$ being phenomenologically introduced for the damping and dephasing of the excited state. Here, $\Delta_{fi} = (E_f - E_i)/\hbar$ is the transition frequency between the initial state $|i\rangle$ and the final state $|f\rangle$. Therefore, the induced electric dipole can be rewritten as

$$\langle\vec{d}\rangle = -\vec{E}_0\mathrm{Re}\sum_{i,f}\rho_i\left(\frac{\vec{d}_{if}\vec{d}_{fi}e^{-i\omega t}}{\omega - \Delta_{fi} + i\gamma} - \frac{\vec{d}_{if}\vec{d}_{fi}e^{-i\omega t}}{\omega + \Delta_{fi} + i\gamma}\right). \tag{B12}$$

Under the rotating-wave approximation [86], the second term of the above equation should be neglected, i.e.,

$$\langle\vec{d}\rangle \approx -\vec{E}_0\ \mathrm{Re}\sum_{i,f}\left(\frac{\rho_i\vec{d}_{if}\vec{d}_{fi}}{\omega - \Delta_{fi} + i\gamma}e^{-i\omega t}\right). \tag{B13}$$

Assuming that all NV centers are identical, the polarization density reads

$$\vec{P} = \frac{n_0}{\hbar}\langle\vec{d}\rangle, \tag{B14}$$

where n_0 is the density of the NV centers in diamond.

Appendix C: Lorentz Local-Field Theory

According to Ref. [70], in closely-packed molecules the polarization of neighboring molecules gives rise to an internal field $\vec{E}_i$ at any molecule, in addition to the external field $\vec{E}$. The internal field is

$$\vec{E}_i = \vec{E}_{\mathrm{near}} - \vec{E}_{\mathrm{mean}}, \tag{C1}$$

where $\vec{E}_{\mathrm{near}}$ is the actual contribution from the molecules close to the given molecule, and $\vec{E}_{\mathrm{mean}}$ is the contribution from those molecules treated in an average continuum. As proven in Ref. [70], in any crystal structure $\vec{E}_{\mathrm{near}} = 0$ due to symmetry, and thus $\vec{E}_i = -\vec{E}_{\mathrm{mean}}$.

By dipole approximation and assuming no net charge in the volume V, the mean-field contribution is [70]

$$\vec{E}_{\mathrm{mean}} = -(\varepsilon_{\mathrm{D}} - 1)\vec{E} - \frac{1}{3V\varepsilon_0}\sum_l \vec{d}_l, \tag{C2}$$

where $\varepsilon_{\mathrm{D}} = 5.7$ is relative permittivity of diamond [76], and the second term is summed over all induced molecular electric dipole moments $\vec{d}_l$ within the volume. Under the weak field approximation, the induced dipole moment is

$$\vec{p}_l = \varepsilon_0\gamma_{\mathrm{mol}}(\vec{E} + \vec{E}_i), \tag{C3}$$

where γ_{mol} is generally a second-order tensor. Since $\vec{E}_i = (\varepsilon_{\mathrm{D}} - 1)\vec{E} + \vec{P}/(3\varepsilon_0)$ [70, 87], the polarization $\vec{P} \equiv \sum_l \vec{d}_l/V = n_0\vec{d}_l$ reads

$$\vec{P} = n_0\varepsilon_0\gamma_{\mathrm{mol}}(\vec{E} + \vec{E}_i) = n_0\varepsilon_0\gamma_{\mathrm{mol}}(\varepsilon_{\mathrm{D}}\vec{E} + \frac{\vec{P}}{3\varepsilon_0}). \tag{C4}$$

Furthermore, using $\vec{P} = \varepsilon_0 \chi_e \vec{E}$ [70, 87], we have

$$\varepsilon_0 \chi_e \vec{E} = n_0 \varepsilon_0 \gamma_{\rm mol} (\varepsilon_{\rm D} + \frac{\chi_e}{3}) \vec{E}, \tag{C5}$$

leading to

$$\chi_e = \frac{n_0 \gamma_{\rm mol} \varepsilon_{\rm D}}{1 - \frac{1}{3} n_0 \gamma_{\rm mol}}. \tag{C6}$$

In diamond with NV centers aligned in the same direction, $\gamma_{\rm mol}$ is of the form

$$\gamma_{\rm mol} = \begin{pmatrix} \eta(\omega)/n_0 & 0 & 0 \\ 0 & 0 & 0 \\ 0 & 0 & 0 \end{pmatrix}, \tag{C7}$$

where $\eta(\omega)$ is the second part of Eq. (4). Therefore, the electric susceptibility is

$$\chi_e = \begin{pmatrix} \frac{3\varepsilon_{\rm D}\eta}{3-\eta} & 0 & 0 \\ 0 & 0 & 0 \\ 0 & 0 & 0 \end{pmatrix}, \tag{C8}$$

and the relative permittivity is

$$\overleftrightarrow{\varepsilon_r} = \begin{pmatrix} \varepsilon_{\rm D}(1 + \frac{3\eta}{3-\eta}) & 0 & 0 \\ 0 & \varepsilon_{\rm D} & 0 \\ 0 & 0 & \varepsilon_{\rm D} \end{pmatrix}. \tag{C9}$$

The frequency domain of the negative refraction is determined by the two solutions to the equation

$$\frac{3}{2} + \eta = 0, \tag{C10}$$

which is not qualitatively different from the equation for the case without the local-field correction

$$\varepsilon_{\rm D} + \eta = 0. \tag{C11}$$

As a result, both the center and bandwidth of the negative refraction in the frequency domain are not substantially modified by the Lorentz local-field correction. This is in consistent with the numerical results in Refs. [10, 78, 79].

Appendix D: Non-Hermitian Hamiltonian Approach

The dynamics of the open quantum system can be described by the Lindblad-form quantum master equation [88]

$$\frac{d\rho}{dt} = -i\,[H, \rho] + \frac{\gamma}{2} \sum_j (2A_j \rho A_j^\dagger - A_j^\dagger A_j \rho - \rho A_j^\dagger A_j), \tag{D1}$$

where A_j's are the excited states projection operators, and γ is the rate of damping and dephasing of the excited states. Equation (D1) can be rewritten as

$$\frac{d\rho}{dt} = -i(H_{\rm cond}\rho - \rho H_{\rm cond}^\dagger) + \gamma \sum_j A_j \rho A_j^\dagger \tag{D2}$$

with

$$H_{\rm cond} = H - i\frac{\gamma}{2} \sum_j A_j^\dagger A_j. \tag{D3}$$

When the typical process of H is much faster than the decoherence process, i.e., the smallest energy gap of H is far greater than γ, the last term of Eq. (D2) can be ignored and thus

$$\frac{d\rho}{dt} = -i\left(H_{\rm cond}\rho - \rho H_{\rm cond}^\dagger\right). \tag{D4}$$

In other words, the decoherence effects could be accounted by solving Schrödinger equation with a non-Hermitian Hamiltonian (D3), instead of solving the quantum master equation. This technique has been widely used in the study of open quantum systems and quantum chemistry, e.g. avian navigation [89] and exciton energy transfer in photosynthesis [90].

[1] V. G. Veselago, The electrodynamics of substances with simultaneously negative values of ε and μ, Sov. Phys. Uspekhi. **10**, 509 (1968).

[2] J. B. Pendry, Negative refraction makes a perfect lens, Phys. Rev. Lett. **85**, 3966 (2000).

[3] D. R. Smith, W. J. Padilla, D. C. Vier, S. C. Nemat-Nasser, and S. Schultz, Composite medium with simultaneously negative permeability and permittivity, Phys. Rev. Lett. **84**, 4184 (2000).

[4] K. Y. Bliokh, Y. P. Bliokh, V. Freilikher, S. Savel'ev, and F. Nori, Colloquium: Unusual resonators: Plasmonics, metamaterials, and random media, Rev. Mod. Phys. **80**, 1201 (2008).

[5] R. K. Zhao, Y. Luo, and J. B. Pendry, Transformation optics applied to van der Waals interactions, Sci. Bull. **61**, 59 (2016).

[6] Y. Shen and Q. Ai, Optical properties of drug metabolites in latent fingermarks, Sci. Rep. **6**, 20336 (2016).

[7] Y. P. Bliokh, V. Freilikher, and F. Nori, Ballistic charge transport in graphene and light propagation in periodic dielectric structures with metamaterials: A comparative study, Phys. Rev. B **87**, 245134 (2013).

[8] A. V. Kats, S. Savel'ev, V. A. Yampol'skii, and F. Nori, Left-handed interfaces for electromagnetic surface waves,

Phys. Rev. Lett. **98**, 073901 (2007).
[9] J. Yao, Z. Liu, Y. Liu, Y. Wang, C. Sun, G. Bartal, A. M. Stacy, and X. Zhang, Optical negative refraction in bulk metamaterials of nanowires, Science **321**, 930 (2008).
[10] Y. N. Fang, Y. Shen, Q. Ai, and C. P. Sun, Negative refraction in Möbius molecules, Phys. Rev. A **94**, 043805 (2016).
[11] J. X. Zhao, J. J. Cheng, Y. Q. Chu, Y. X. Wang, F. G. Deng, and Q. Ai, Hyperbolic metamaterial using chiral molecules, Sci. China-Phys. Mech. Astron. **63**, 260311 (2020).
[12] C. W. Chang, M. Liu, S. Nam, S. Zhang, Y. Liu, G. Bartal, and X. Zhang, Optical Möbius symmetry in metamaterials, Phys. Rev. Lett. **105**, 235501 (2010).
[13] Y. Shen, H. Y. Ko, Q. Ai, S. M. Peng, and B. Y. Jin, Molecular split-ring resonators based on metal string complexes, J. Phys. Chem. C **118**, 3766 (2014).
[14] A. L. Rakhmanov, V. A. Yampol'skii, J. A. Fan, F. Capasso, and F. Nori, Layered superconductors as negative-refractive-index metamaterials, Phys. Rev. B **81**, 075101 (2010).
[15] A. Poddubny, I. Iorsh, P. Belov, and Y. Kivshar, Hyperbolic metamaterials, Nat. Photon. **7**, 958 (2013).
[16] S. Jahani and Z. Jacob, All-dielectric metamaterials, Nat. Nanotechnol. **11**, 23 (2016).
[17] D. R. Smith and D. Schurig, Electromagnetic wave propagation in media with indefinite permittivity and permeability tensors, Phys. Rev. Lett. **90**, 077405 (2003).
[18] P. A. Belov, Backward waves and negative refraction in uniaxial dielectrics with negative dielectric permittivity along the anisotropy axis, Microw. Opt. Technol. Lett. **37**, 259 (2003).
[19] Z. Liu, H. Lee, Y. Xiong, C. Sun, and X. Zhang, Far-field optical hyperlens magnifying sub-diffraction-limited objects, Science **315**, 1686 (2007).
[20] S. Ishii, A. V. Kildishev, E. Narimanov, V. M. Shalaev, and V. P. Drachev, Sub-wavelength interference pattern from volume plasmon polaritons in a hyperbolic medium, Las. Photon. Rev. **7**, 265 (2013).
[21] Z. Jacob, I. Smolyaninov, and E. Narimanov, Broadband Purcell effect: Radiative decay engineering with metamaterials, Appl. Phys. Lett. **100**, 181105 (2012).
[22] S. A. Biehs, M. Tschikin, and P. Ben-Abdallah, Hyperbolic metamaterials as an analog of a blackbody in the near field, Phys. Rev. Lett. **109**, 104301 (2012).
[23] J. Li, L. Fok, X. Yin, G. Bartal, and X. Zhang, Experimental demonstration of an acoustic magnifying hyperlens, Nat. Mater. **8**, 931 (2009).
[24] I. I. Smolyaninov and E. E. Narimanov, Metric signature transitions in optical metamaterials, Phys. Rev. Lett. **105**, 067402 (2010).
[25] H. N. S. Krishnamoorthy, Z. Jacob, E. Narimanov, I. Kretzschmar, and V. M. Menon, Topological transitions in metamaterials, Science **336**, 205 (2012).
[26] X. Yang, J. Yao, J. Rho, X. Yin, and X. Zhang, Experimental realization of three-dimensional indefinite cavities at the nanoscale with anomalous scaling laws, Nat. Photon. **6**, 450 (2012).
[27] R. Schirhagl, K. Chang, M. Loretz, and C. L. Degen, Nitrogen-vacancy centers in diamond: Nanoscale sensors for physics and biology, Annu. Rev. Phys. Chem. **65**, 83 (2014).
[28] Y. Wu, F. Jelezko, M. B. Plenio, and T. Weil, Diamond quantum devices in biology, Angew. Chem. Int. Ed. **55**, 6586 (2016).
[29] M. W. Doherty, N. B. Manson, P. Delaney, F. Jelezko, J. Wrachtrup, and L. C. L. Hollenberg, The nitrogen-vacancy colour centre in diamond, Phys. Rep. **528**, 1 (2013).
[30] M. Chen, C. Meng, Q. Zhang, C. Duan, F. Shi, and J. F. Du, Quantum metrology with single spins in diamond under ambient conditions, Natl. Sci. Rev. **5**, 2095 (2018).
[31] J. Jeske, D. W. M. Lau, X. Vidal, L. P. McGuinness, P. Reineck, B. C. Johnson, M. W. Doherty, J. C. McCallum, S. Onoda, F. Jelezko, T. Ohshima, T. Volz, J. H. Cole, B. C. Gibson, and A. D. Greentree, Stimulated emission from nitrogen-vacancy centres in diamond, Nat. Commun. **8**, 14000 (2017).
[32] L. Jin, M. Pfender, N. Aslam, P. Neumann, S. Yang, J. Wrachtrup, and R.-B. Liu, Proposal for a room-temperature diamond maser, Nat. Commun. **6**, 8251 (2015).
[33] M. P. Ledbetter, K. Jensen, R. Fischer, A. Jarmola, and D. Budker, Gyroscopes based on nitrogen-vacancy centers in diamond, Phys. Rev. A **86**, 052116 (2012).
[34] B. B. Zhou, A. Baksic, H. Ribeiro, C. G. Yale, F. J. Heremans, P. C. Jerger, A. Auer, G. Burkard, A. A. Clerk, and D. D. Awschalom, Accelerated quantum control using superadiabatic dynamics in a solid-state lambda system, Nat. Phys. **13**, 330 (2017).
[35] X. K. Song, Q. Ai, J. Qiu, and F. G. Deng, Physically feasible three-level transitionless quantum driving with multiple Schrödinger dynamics, Phys. Rev. A **93**, 052324 (2016).
[36] F. Dolde, H. Fedder, M. W. Doherty, T. Nobauer, F. Rempp, G. Balasubramanian, T. Wolf, F. Reinhard, L. C. L. Hollenberg, F. Jelezko, and J. Wrachtrup, Electric-field sensing using single diamond spins, Nat. Phys. **7**, 459 (2011).
[37] F. Dolde, M. W. Doherty, J. Michl, I. Jakobi, B. Naydenov, S. Pezzagna, J. Meijer, P. Neumann, F. Jelezko, N. B. Manson, and J. Wrachtrup, Nanoscale detection of a single fundamental charge in ambient conditions using the NV^- center in diamond, Phys. Rev. Lett. **112**, 097603 (2014).
[38] J. R. Maze, P. L. Stanwix, J. S. Hodges, S. Hong, J. M. Taylor, P. Cappellaro, L. Jiang, M. V. G. Dutt, E. Togan, A. S. Zibrov, A. Yacoby, R. L. Walsworth, and M. D. Lukin, Nanoscale magnetic sensing with an individual electronic spin in diamond, Nature (London) **455**, 644 (2008).
[39] G. Balasubramanian, I. Y. Chan, R. Kolesov, M. Al-Hmoud, J. Tisler, C. Shin, C. Kim, A. Wojcik, P. R. Hemmer, A. Krueger, T. Hanke, A. Leitenstorfer, R. Bratschitsch, F. Jelezko, and J. Wrachtrup, Nanoscale imaging magnetometry with diamond spins under ambient conditions, Nature (London) **455**, 648 (2008).
[40] Y. Liu, F. Kong, F. Z. Shi, and J. F. Du, Detection of radio-frequency field with a single spin in diamond, Sci. Bull. **61**, 1132 (2016).
[41] L. S. Li, H. H. Li, L. L. Zhou, Z. S. Yang, and Q. Ai, Measurement of weak static magnetic fields with nitrogen-vacancy color center, Acta. Phys. Sin. **66**, 230601 (2017).
[42] N. Zhao, J.-L. Hu, S.-W. Ho, T.-K. Wen, and R. B. Liu, Atomic-scale magnetometry of distant nuclear spin clusters via nitrogen-vacancy spin in diamond, Nat. Nanotechnol. **6**, 242 (2011).

[43] Z. S. Yang, Y. X. Wang, M. J. Tao, W. Yang, M. Zhang, Q. Ai, and F. G. Deng, Longitudinal relaxation of a nitrogen-vacancy center in a spin bath by generalized cluster-correlation expansion method, Ann. Phys. **413**, 168063 (2020).

[44] M. S. Grinolds, S. Hong, P. Maletinsky, L. Luan, M. D. Lukin, R. L. Walsworth, and A. Yacoby, Nanoscale magnetic imaging of a single electron spin under ambient conditions, Nat. Phys. **9**, 215 (2013).

[45] A. Cooper, E. Magesan, H. Yum, and P. Cappellaro, Time-resolved magnetic sensing with electronic spins in diamond, Nat. Commun. **5**, 3141 (2014).

[46] F. Shi, Q. Zhang, P. Wang, H. Sun, J. Wang, X. Rong, M. Chen, C. Ju, F. Reinhard, H. Chen, J. Wrachtrup, J. Wang, and J. F. Du, Single-protein spin resonance spectroscopy under ambient conditions, Science **347**, 1135 (2015).

[47] S. J. DeVience, L. M. Pham, I. Lovchinsky, A. O. Sushkov, N. Bar-Gill, C. Belthangady, F. Casola, M. Corbett, H. Zhang, M. Lukin, H. Park, A. Yacoby, and R. L. Walsworth, Nanoscale NMR spectroscopy and imaging of multiple nuclear species, Nat. Nanotechnol. **10**, 129 (2015).

[48] J. M. Boss, K. Chang, J. Armijo, K. Cujia, T. Rosskopf, J. R. Maze, and C. L. Degen, One- and two-dimensional nuclear magnetic resonance spectroscopy with a diamond quantum sensor, Phys. Rev. Lett. **116**, 197601 (2016).

[49] H. B. Liu, M. B. Plenio, and J.-M. Cai, Scheme for detection of single-molecule radical pair reaction using spin in diamond, Phys. Rev. Lett. **118**, 200402 (2017).

[50] Y.-Y. Wang, J. Qiu, Y.-Q. Chu, M. Zhang, J.-M. Cai, Q. Ai, and F.-G. Deng, Dark state polarizing a nuclear spin in the vicinity of a nitrogen-vacancy center, Phys. Rev. A **97**, 042313 (2017).

[51] G. Kucsko, P. C. Maurer, N. Y. Yao, M. Kubo, H. J. Noh, P. K. Lo, H. Park, and M. D. Lukin, Nanometre-scale thermometry in a living cell, Nature (London) **500**, 54 (2013).

[52] D. M. Toyli, C. F. de las Casas, D. J. Christle, V. V. Dobrovitski, and D. D. Awschalom, Fluorescence thermometry enhanced by the quantum coherence of single spins in diamond, Proc. Natl. Acad. Sci. U.S.A. **110**, 8417 (2013).

[53] P. Neumann, I. Jakobi, F. Dolde, C. Burk, R. Reuter, G. Waldherr, J. Honert, T. Wolf, A. Brunner, J. H. Shim, D. Suter, H. Sumiya, J. Isoya, and J. Wrachtrup, High-precision nanoscale temperature sensing using single defects in diamond, Nano Lett. **13**, 2738 (2013).

[54] Z.-L. Xiang, S. Ashhab, J. Q. You, and F. Nori, Hybrid quantum circuits: Superconducting circuits interacting with other quantum systems, Rev. Mod. Phys. **85**, 623 (2013).

[55] Z.-L. Xiang, X.-Y. Lü, T.-F. Li, J. Q. You, and F. Nori, Hybrid quantum circuit consisting of a superconducting flux qubit coupled to a spin ensemble and a transmission-line resonator, Phys. Rev. B **87**, 144516 (2013).

[56] X.-Y. Lü, Z.-L. Xiang, W. Cui, J. Q. You, and F. Nori, Quantum memory using a hybrid circuit with flux qubits and nitrogen-vacancy centers, Phys. Rev. A **88**, 012329 (2013).

[57] P.-B. Li, Z.-L. Xiang, P. Rabl, and F. Nori, Hybrid quantum device with nitrogen-vacancy centers in diamond coupled to carbon nanotubes, Phys. Rev. Lett. **117**, 015502 (2016).

[58] K. Cai, R. X. Wang, Z. Q. Yin, and G. L. Long, Second-order magnetic field gradient-induced strong coupling between nitrogen-vacancy centers and a mechanical oscillator, Sci. China-Phys. Mech. Astron. **60**, 070311 (2017).

[59] A. M. Zagoskin, J. R. Johansson, S. Ashhab, and F. Nori, Quantum information processing using frequency control of impurity spins in diamond, Phys. Rev. B **76**, 014122 (2007).

[60] E. van Oort and M. Glasbeek, Electric-field-induced modulation of spin echoes of N-V centers in diamond, Chem. Phys. Lett. **168**, 529 (1990).

[61] A. Batalov, V. Jacques, F. Kaiser, P. Siyushev, P. Neumann, L. J. Rogers, R. L. McMurtrie, N. B. Manson, F. Jelezko, and J. Wrachtrup, Low temperature studies of the excited-state structure of negatively charged nitrogen-vacancy color centers in diamond, Phys. Rev. Lett. **102** 195506 (2009).

[62] N. R. S. Reddy, N. B. Manson, and E. R. Krausz, Two-laser spectral hole burning in a color center in diamond, J. Lumin **38**, 46 (1987).

[63] L. J. Rogers, R. L. McMurtie, M. J. Sellars, and N. B. Manson, Time-averaging within the excited state of the nitrogen-vacancy centre in diamond, New J. Phys. **11**, 063007 (2009).

[64] G. D. Fuchs, V. V. Dobrovitski, R. Hanson, A. Batra, C. D. Weis, T. Schenkel, and D. D. Awschalom, Excited-state spectroscopy using single spin manipulation in diamond, Phys. Rev. Lett. **101**, 117602 (2008).

[65] P. Neumann, R. Kolesov, V. Jacques, J. Beck, J. Tisler, A. Batalov, L. Rogers, N.B. Manson, G. Balasubramanian, F. Jelezko, and J. Wrachtrup, Excited-state spectroscopy of single NV defects in diamond using optically detected magnetic resonance, New J. Phys. **11**, 013017 (2009).

[66] Ph. Tamarat, N. B. Manson, J. P. Harrison, R. L. McMurtrie, A. Nizovtsev, C. Santori, R. G. Beausoleil, P. Neumann, T. Gaebel, F. Jelezko, P. Hemmer, and J. Wrachtrup, Spin-flip and spin-conserving optical transitions of the nitrogen-vacancy centre in diamond, New J. Phys. **10**, 045004 (2008).

[67] Ph. Tamarat, T. Gaebel, J. R. Rabeau, M. Khan, A. D. Greentree, H. Wilson, L. C. L. Hollenberg, S. Prawer, P. Hemmer, F. Jelezko, and J. Wrachtrup, Stark shift control of single optical centers in diamond, Phys. Rev. Lett. **97**, 083002 (2006).

[68] L. J. Zou, D. Marcos, S. Diehl, S. Putz, J. Schmiedmayer, J. Majer, and P. Rabl, Implementation of the Dicke lattice model in hybrid quantum system arrays, Phys. Rev. Lett. **113**, 023603 (2014).

[69] J. R. Maze, A. Gali, E. Togan, Y. Chu, A. Trifonov, E. Kaxiras, and M. D. Lukin, Properties of nitrogen-vacancy centers in diamond: The group theoretic approach, New J. Phys. **13**, 025025 (2011).

[70] J. D. Jackson, *Classical Electrodynamics* 3rd ed., (John Wiley, United States, 1999).

[71] L. D. Landau, E. M. Lifshitz, and L. P. Pitaevskii, *Electrodynamics of Continuous Media* 2nd Ed., (Butterworth Heinmann, Oxford, 1995).

[72] R. Kubo, M. Toda, and N. Hashitsume, *Statistical Physics II Nonequilibrium Statistical Mechanics* (Springer-Verlag, Berlin Heidelberg, 1985).

[73] J. Choi, S. Choi, G. Kucsko, P. C. Maurer, B. J. Shields, H. Sumiya, S. Onoda, J. Isoya, E. Demler, F. Jelezko, N. Y. Yao, and M. D. Lukin, Depolarization dynamics

in a strongly interacting solid-state spin ensemble, Phys. Rev. Lett. **118**, 093601 (2017).

[74] K.-M. C. Fu, C. Santori, P. E. Barclay, L. J. Rogers, N. B. Manson, and R. G. Beausoleil, Observation of the dynamic Jahn-Teller effect in the excited states of nitrogen-vacancy centers in diamond, Phys. Rev. Lett. **103**, 256404 (2009).

[75] A. Lenef, S. W. Brown, D. A. Redman, and S. C. Rand, Electronic structure of the N-V center in diamond: Experiments, Phys. Rev. B **53**, 13427 (1996).

[76] J. Fontanella, R. L. Johnston, J. H. Colwell, and C. Andeen, Temperature and pressure variation of the refractive index of diamond, Appl. Opt. **16**, 2949 (1977).

[77] H. D. Young, *University Physics* 7th Ed., (Addison Wesley, San Francisco, 1992).

[78] J. Kästel, M. Fleischhauer, S. F. Yelin, and R. L. Walsworth, Tunable negative refraction without absorption via electromagnetically induced chirality, Phys. Rev. Lett. **99**, 073602 (2007).

[79] J. Kästel, M. Fleischhauer, and G. Juzeliūnas, Local-field effects in magnetodielectric media: Negative refraction and absorption reduction, Phys. Rev. A **76**, 062509 (2007).

[80] T. Suto, J. Yaita, T. Iwasaki, and M. Hatano, Highly oriented diamond (111) films synthesized by pulse bias-enhanced nucleation and epitaxial grain selection on a 3C-SiC/Si (111) substrate, Appl. Phys. Lett. **110**, 062102 (2017).

[81] A. Jarmola, V. M. Acosta, K. Jensen, S. Chemerisov, and D. Budker, Temperature- and magnetic-field-dependent longitudinal spin relaxation in nitrogen-vacancy ensembles in diamond, Phys. Rev. Lett. **108**, 197601 (2012).

[82] P. Kehayias, M. J. Turner, R. Trubko, J. M. Schloss, C. A. Hart, M. Wesson, D. R. Glenn, and R. L. Walsworth, Imaging crystal stress in diamond using ensembles of nitrogen-vacancy centers, Phys. Rev. B **100,** 174103 (2019).

[83] M. W. Doherty, N. B. Manson, P. Delaney, and L. C. L. Hollenberg, The negatively charged nitrogen-vacancy centre in diamond: The electronic solution, New J. Phys. **13**, 025019 (2011).

[84] E. Togan, Y. Chu, A. S. Trifonov, L. Jiang, J. Maze, L. Childress, M. V. G. Dutt, A. S. Sørensen, P. R. Hemmer, A. S. Zibrov, and M. D. Lukin, Quantum entanglement between an optical photon and a solid-state spin qubit, Nature (London) **466**, 730 (2010).

[85] J. J. Sakurai, *Modern Quantum Mechanics* (Addison-Wesley, Reading, MA, 1993).

[86] Q. Ai, Y. Li, H. Zheng, and C. P. Sun, Quantum anti-Zeno effect without rotating wave approximation, Phys. Rev. A **81**, 042116 (2010).

[87] R. Marqués, F. Martín, and M. Sorolla, *Metamaterials with Negative Parameters: Theory, Design and Microwave Applications* (John Wiley, New Jersey, 2008).

[88] H.-P. Breuer and F. Petruccione, *The Theory of Open Quantum Systems* (Oxford University Press, 2007).

[89] I. K. Kominis, Quantum Zeno effect explains magnetic-sensitive radical-ion-pair reactions, Phys. Rev. E **80**, 056115 (2009).

[90] A. Olaya-Castro, C. F. Lee, F. F. Olsen, and N. F. Johnson, Efficiency of energy transfer in a light-harvesting system under quantum coherence, Phys. Rev. B **78,** 085115 (2008).